EUROPEAN ORGANIZATION FOR NUCLEAR RESEARCH

THE REACTIONS $\pi^- p \to \rho^0 n$ AND $K^- p \to K^{*0}(890) n$ AT 11.2 GeV/c

B.D. Hyams, W. Koch*), D.C. Potter and J.D. Wilson,
CERN, Geneva, Switzerland

and

L. Von Lindern, E. Lorenz, G. Lütjens, U. Stierlin and P. Weilhammer,
Max-Planck-Institut für Physik und Astrophysik, Munich, Germany.

ABSTRACT

We report here the results of a spark chamber experiment in which the reactions $\pi^- p \to \rho^0 n$ and $K^- p \to K^{*0}(890) n$ were studied at 11.2 GeV/c incident beam momentum. The cross-sections are determined to be $\sigma(\rho^0) = 128 \pm 16$ μb and $\sigma[K^{*0}(890)] = 53 \pm 8$ μb. Differential cross-sections and values of the spin density matrix elements are given for both reactions. An enhancement in the $(\pi^- \pi^+)$ invariant mass distribution is observed at a mass of 945 MeV.

Geneva - 5 July 1968
(Submitted to Nuclear Physics)

---

*) Now at the Max-Planck-Institut für Physik und Astrophysik, Munich, Germany.

THE REACTIONS $\pi^- p \to \rho^0 n$ AND $K^- p \to K^{*0}(890) n$ AT 11.2 GeV/c

B.D. Hyams, W. Koch*), D.C. Potter and J.D. Wilson,
CERN, Geneva, Switzerland

and

L. Von Lindern, E. Lorenz, G. Lütjens, U. Stierlin and P. Weilhammer,
Max-Planck-Institut für Physik und Astrophysik, Munich, Germany.

1. INTRODUCTION

The reactions

$$\pi^- + p \to \rho^0 + n \qquad (1)$$
$$\hookrightarrow \pi^- + \pi^+$$

and

$$K^- + p \to K^{*0}(890) + n \qquad (2)$$
$$\hookrightarrow K^- + \pi^+$$

have been studied previously[1-9] at several beam energies. Existing data, however, are somewhat scant in the region of 11 GeV/c. For this reason we made slight modifications to an experimental apparatus already operating at the CERN Proton Synchrotron[10], thus attempting to select reactions (1) and (2). We obtained 2250 events fitting the reaction

$$\pi^- + p \to \pi^- + \pi^+ + n \qquad (3)$$

and 290 events of the type

$$K^- + p \to K^- + \pi^+ + n \,. \qquad (4)$$

---

*) Now at the Max-Planck-Institut für Physik und Astrophysik, Munich, Germany.

Our results on the production cross-sections and the production and decay angular distributions are compared with the predictions of the one-pion exchange model with absorption (OPEA)[11].

2. EXPERIMENTAL ARRANGEMENT

The experimental arrangement is shown schematically in Fig. 1. The beam (defined by a coincidence $A\,B\,\bar{C}$) was momentum analysed in optical spark chambers S1-S4 and the 2 metre bending magnet M1. The secondary particles emanating from the 1 metre liquid-hydrogen target were detected by counter arrays G and E (consisting of a number of scintillators 140 cm in height) and their momenta were determined in optical spark chambers S5-S8 and spectrometer magnet M2 (15.5 kGm, 100 × 100 × 50 cm^3). Anti-counter D signified the interaction of a beam particle in the target. Anticounters F were placed around the sides of the target, together with lead sheets, in an effort to reject interactions with charged particles and γ rays leaving the target in a lateral direction. Rejection of this type of interaction was improved with the aid of anticounters H5-H8, a lead and scintillator arrangement defining the aperture of M2. Furthermore, the pole faces of M2 were shielded with more anticounters H1-H4. The trigger condition for the spark chambers was an interacting beam particle in coincidence with two (and only two) counter signals from each of the arrays G and E, but no pulse from any F or H counter.

Two threshold Čerenkov counters were employed to signify each beam particle as a π^-(μ or e), K^-, or $\bar{p}$. For most of the beam burst length we allowed only K^- triggers, but if none was obtained we accepted a π^- trigger towards the end of the spill. In this way we accumulated photographs of 30,000 π events and 10,000 K events.

By means of a large mirror arrangement, two views of each chamber (90° stereoscopy) were recorded on a single frame at a demagnification of ~ 40. To facilitate the pairing of the track segments in the two stereoscopic views of any chamber, prisms were placed on two of the eight gaps of each side view.

3. FILM MEASUREMENT AND EVENT RECONSTRUCTION

All 40,000 frames were measured by HPD-1 [12] at CERN without any prescanning or preselection; all selection was performed by computer programs at later stages. A GEOMETRY program reconstructed beam and secondary trajectories in space. Tracks in each chamber were defined by two points with a r.m.s. error of ±0.3 mm per point (including the multiple scattering in air and chamber material), the separation of the points being ~ 17 cm. The acceptable reconstructed events were then processed by a KINEMATICS program which used a trajectory-fitting routine (MAGFIT) [13] for momemtum determination in the large spectrometer magnet. We obtained a momentum resolution of ±0.75% for the beam particles and ±0.8% at 5 GeV/c for the secondaries.

For events with only two secondaries of total energy > 10.5 GeV, the combined efficiency of the HPD measurement and the GEOMETRY program was determined to be (91 ± 2)% by comparison with some hand scanning and measurement results. About half of the loss was due to HPD failure in recognizing faint sparks, and about half was the result of the shortcomings of the track pairing by the prisms (owing to optical distortion). This efficiency compares favourably with that of 92%, the mean efficiency of our scanning girls.

Of the 30,000 π events, 7000 were found to have one positively and one negatively charged particle traversing chambers S5-S8; 1500 such events were found for incident K^-.

4. ρ^0 ANALYSIS

For the 7000 π events defined above, we have assumed the two particles to be pions. Figure 2 illustrates the total energy distribution of the $(\pi^-\pi^+)$ system for these events and indicates that our apparatus successfully selected interactions of a peripheral nature. After the application of some geometrical cuts, 2250 events gave a good 1C kinematic fit ($\chi^2 < 4$) to reaction (3) and a missing mass distribution as shown in Fig. 3. Only these events satisfying the kinematic fit were considered in the subsequent analysis. There is some contamination (~ 5%) in Fig. 3 from the reaction $\pi^- p \to \pi^-\pi^+\pi^0 n$, but this has been taken into account in cross-section calculations. The background in this sample due to interaction processes

yielding secondary particles which are not pions has been estimated to be negligible. The absence of such background is partly a consequence of the specific acceptance of our apparatus.

In Fig. 4 we plot the observed $(\pi^-\pi^+)$ mass spectrum the ρ^0 being clearly observed. We have limited the mass scale of Fig. 4 to 1000 MeV because the acceptance of the apparatus for $(\pi^-\pi^+)$ masses greater than this value was less than 10% (to be compared with 50% at 300 MeV). A study of the separation of the $\pi^\pm$ vertex from the beam particle trajectory yielded an unbiased sample of $K^0_S \to \pi^-\pi^+$ decays. These decays gave an absolute calibration of the spectrometer magnet field strength, and directly proved the $(\pi^-\pi^+)$ mass resolution to be ±3.5 MeV. Hence, we calculate the resolution to be ±5.5 MeV at a mass of 770 MeV.

The observed data must be corrected for the limited acceptance of the apparatus. This was achieved by a Monte Carlo procedure determining the acceptance as a function of the four kinematic variables that describe the interaction, namely, the invariant mass $m(\pi^-\pi^+)$, the four-momemtum transfer t, and the decay angles $\Theta(\pi^-)$ and $\Phi(\pi^-)$ of the $(\pi^-\pi^+)$ system defined in the Gottfried-Jackson fame[14]. With the knowledge of the acceptance, we fit the decay angular distribution of the $(\pi^-\pi^+)$ system to its general form (5) in terms of density matrix elements, allowing only for S- and P-waves. With the normalization $2\rho_{11} + \rho_{00} + \rho_{ss} = 1$ we have

$$\left.\begin{aligned} 4\pi\, I(x,\Phi) = 1 &+ (\rho_{00} - \rho_{11})(3x^2 - 1) \\ &- 3\rho_{1\,1}(1 - x^2)\cos 2\Phi - 6\sqrt{2}\ \mathrm{Re}\ \rho_{10}\, x\sqrt{1 - x^2}\cos\Phi \\ &+ 2\sqrt{3}\ \mathrm{Re}\ \rho_{0s}\, x - 2\sqrt{6}\ \mathrm{Re}\ \rho_{1s}\sqrt{1 - x^2}\cos\Phi\ , \end{aligned}\right\} \quad (5)$$

where $x = \cos\Theta(\pi^-)$ and the index s refers to S-wave interference. The S-wave intensity ρ_{ss} cannot in principle be determined from the angular distribution. Fits were obtained for various t and $m(\pi^-\pi^+)$ intervals, all yielding good confidence levels. The results are listed in Table 1 and Fig. 5 depicts the t-dependence of the ρ parameters in the mass region 600-960 MeV. Mention must be made of the fact that for the angular distribution fits, there has been no need for us to remove events with a (πn)

mass in the N*(1236) region, because Dalitz plots show that there are no events with (πn) mass less than 1500 MeV (owing to our limited experimental acceptance).

The fitted decay angular distributions now permit us to correct the observed data for acceptance. In Figure 6 the corrected invariant mass spectrum is plotted for events with $|t| < 0.4$ (GeV/c)^2. Different Breit-Wigner functions with background have been fitted to it, and Table 2 gives a summary of the results. In order to calculate cross-sections, allowances have been made for the measurement and program efficiency, electronic and counter efficiency, muons in the beam, and secondary interactions and decays of pions. Two cross-sections $\sigma(\rho^0)$ for reaction (1) in the interval $|t| < 0.4$ (GeV/c)^2 are quoted in Table 2: σ_1 for 280 < m $\pi(\pi^+)$ < 1000 MeV, and σ_2 for the full kinematic mass range. The cross-section errors given in Table 2 refer only to the uncertainties associated with the fitted ratios of ρ^0 resonance to background. The total error in $\sigma(\rho^0)$, however, must include an experimental error of ±12% which is dominated by an uncertainty in the electronic and counter efficiency.

Figure 7 illustrates the differential cross-sections, $d\sigma/dt'$, for reaction (3) in the ρ^0-mass region (600 to 960 MeV) and in the neighbourhood below (280 to 600 MeV). $t' = t - t_{min}$, where $|t_{min}|$ is the minimum momentum transfer for a given $m(\pi^-\pi^+)$.

5. DISCUSSION OF ρ^0 RESULTS

The variation in $\sigma(\rho^0)$ values of Table 2 indicates some of the difficulties involved when comparing the data of different experiments where no standard fitting procedure has been employed. Nevertheless, we present in Fig. 8 a compilation of $\sigma(\rho^0)$ as a function of p_π, the incident π^- beam laboratory momentum. Our value of 128 ± 16 μb, corresponding to the complete $m(\pi^-\pi^+)$ range, has been taken from fit (A) and has been corrected for the entire t-range (+4% correction). We have simply drawn a line $\sigma(p_\pi) = 14.4\ p_\pi^{-2}$ and have not attempted a rigorous fit for the reason given above. If the true momentum dependence is approximately proportional to p_π^{-2}, our value is consistent with that of Poirier et al.[6] at 8 GeV/c, but not with those of Bellini et al.[7] at 8 and 16 GeV/c.

Besides the more common methods of ρ^0 mass and width determination, we have followed a procedure proposed by Malamud and Schlein[15]. These authors have suggested that, under certain assumptions on the production amplitude, one may project out a pure P-wave part from the $m(\pi^-\pi^+)$ distribution by plotting the moments $N(m)\langle Y_2^M(\Theta,\Phi)\rangle$, where $N(m)$ is the number of events in a bin of mass m, and $\langle Y_2^M\rangle$ is a spherical harmonic Y_2^M averaged over the $(\pi^-\pi^+)$ decay angular distribution in bin m. In Fig. 9 we have plotted $N(m)(\rho_{00}-\rho_{11})$, which is proportional to $N(m)\langle Y_2^0\rangle$. The results of fits to this data of three Breit-Wigner functions without background are given in Table 2 (E, F and G), and fit E is drawn in Fig. 9. Only fit G shows any significant deviation from the corresponding normal fit including background (C).

The experimental differential cross-section for the ρ^0-mass region (Fig. 7) is compared with the theoretical predictions of the OPEA[11]. Two theoretical curves*) have been drawn in Fig. 7. Curve (α) uses $C_1 = 0.62$, $\gamma_1 = 0.012$ (as obtained from πp elastic scattering), $C_2 = 1$, $\gamma_2 = \frac{3}{4}\gamma_1$ (as suggested in Ref. 11), $g^2(\pi^+\pi^-\rho^0)/4\pi = 2$, and $G^2(pn\pi^+)/4\pi = 29.2$; whereas for curve (β) we employ $\gamma_2 = 0.0018$. The theoretical predictions include a correction factor which takes into account the fact that our experimental differential cross-section is limited to the mass region 600 to 960 MeV and contains background (fit A in Table 2). The theoretical cross-section for curve (α) is approximately correct in the region of $|t| < 0.02$ (GeV/c)^2 but not for higher t-values. On the other hand, the prediction for assumption (β) fits the experimental slope rather well but there is a discrepancy of about a factor of 1.6 in magnitude. The experimental $d\sigma/dt'$ for the lower mass region illustrates essentially the same t-dependence as for the ρ^0-mass region, except for the decrease at very small t-values. For the ρ^0-mass region and $0.02 < |t'| < 0.12$ (GeV/c)^2, the differential cross-section can be well approximated by the exponential form $d\sigma/dt' = Ae^{-\lambda t'}$ with $\lambda = 16.2$ (GeV/c)$^{-2}$.

The OPEA predictions have also been tested by considering the t-dependence of the ρ parameters, in the central ρ^0-mass region. The theoretical curves*) drawn in Fig. 5 correspond to assumption (α) which

---

*) The OPEA predictions were computed by means of a program written by R. Keyser.

does not include S-wave (i.e. $\rho_{ss} = 0$); qualitative agreement is obtained. As expected from OPEA, the t-dependences of $(\rho_{00}-\rho_{11})$, ρ_{1-1}, and Re ρ_{10} at our energy are essentially the same as those found at lower energies[2,6]. The same is true for the "forward-backward asymmetry" in the ρ^0 decay which is related to Re ρ_{0s} by

$$(F - B)/(F + B) = \sqrt{3}\ \text{Re}\ \rho_{0s}\ ,$$

under the assumption of only S- and P-wave interference.

We consider that we do not have sufficient data to make a reliable $\pi\pi$ phase-shift analysis, but in Table 1 we have indicated the mass dependence of the ρ parameters for $0 < |t| < 0.2$ (GeV/c)^2.

Inspection of Figs. 4 and 6 reveals a peak at an invariant mass of $\sim$ 945 MeV where the mass resolution is ±6.5 MeV. For the weighted data, the peak is at least 4.5 standard deviations above all the fitted Breit-Wigner plus background distributions extended to 970 MeV. We cannot explain this rather narrow peak as being due to a bias in our apparatus or analysis, nor as a misinterpretation of the decay of a known particle. No previous reports have been published concerning such a "resonance" in the $m(\pi^-\pi^+)$ distribution, but our rather good mass resolution should be noted.

6. $K^{*0}(890)$ ANALYSIS AND DISCUSSION

After the removal of events fitting $K^-p \to K^0n$ $(K^0 \to \pi^-\pi^+)$, the analysis of events with an incident K^- was analogous to that described in Section 4 for π events, except that the secondary particles were assumed to be K^- and π^+. Figure 10 shows the unweighted invariant $(K^-\pi^+)$ mass distribution of those events (278) fitting reaction (4) with $\chi^2 < 4$ and $|t| < 0.4$ (GeV/c)^2. The decay angular distribution was fitted to Eq. (5) in the range $790 < m(K^-\pi^+) < 990$ MeV, and hence the experimental acceptance in this region was determined together with the cross-section for reaction (2). A constant width Breit-Wigner of mass 893 MeV and width 49 MeV with linear background was fitted to the data. The following results were obtained for the intervals $|t| < 0.4$ (GeV/c)^2 and $790 < m(K^-\pi^+) < 990$ MeV, with background subtraction and partial decay mode correction having been made for the cross-section:

$$\sigma[K^*(890)] = 53 \pm 8\ \mu b$$

$$(\rho_{00}-\rho_{11}) = 0.374 \pm 0.081\ (0.54)$$

$$\rho_{1-1} = 0.040 \pm 0.034\ (0.062)$$

$$\text{Re}\ \rho_{10} = -0.143 \pm 0.026\ (-0.175)$$

$$\text{Re}\ \rho_{0S} = 0.191 \pm 0.042$$

$$\text{Re}\ \rho_{1S} = -0.047 \pm 0.023$$

In Fig. 11 we plot the differential cross-section for the $K^{*0}(890)$ mass region. Since previous experiments[8,9] have shown that $K^{*0}(890)$ production involves predominantly a single pion exchange, we have drawn in Fig. 11 the theoretical $d\sigma/dt'$ following from the parameters $C_1 = 0.52$, $\gamma_1 = 0.012$, $C_2 = 1.0$, $\gamma_2 = 0.009$, $g^2(\pi^+K^-K^{*0})/4\pi = 1.65$, and $G^2(pn\pi^+)/4\pi = 29.2$ in the OPEA. The ρ-parameter values quoted in brackets are the theoretical values for the above OPEA parameters.

Our results for $K^{*0}(890)$ production and decay exhibit no significant differences from the data of other experiments.

* * *

Acknowledgements

We are indebted for the effort of members of the CERN Data Handling Division involved with the HPD measurements. We would like to thank the Machine Division of the CERN Proton Synchrotron for their able assistance in all phases of the experiment. We thank Professors B. Gregory, W. Heisenberg, W. Paul and P. Preiswerk for their continued support.

REFERENCES

1) T.C. Bacon, W.J. Fickinger, D.G. Hill, H.W.K. Hopkings, D.K. Robinson and E.O. Salant, Phys.Rev. 157, 1263 (1967).

2) L.D. Jacobs (Thesis) UCRL-16877 (unpublished).

3) D.H. Miller, L. Gutay, P.B. Johnson, F.J. Loeffler, R.L. McIlwain, R.J. Spzafka and R.B. Willmann, Phys.Rev. 153, 1423 (1967).

4) Aachen-Birmingham-Bonn-Hamburg-London (I.C.)-München Collaboration. Nuovo Cimento 31, 729 (1964).
I. Derado, V.P. Kenney, J.A. Poirier and W.D. Shephard, Phys.Rev. Letters 14, 872 (1965).

5) R.L. Eisner, P.B. Johnson, P.R. Klein, R.E. Peters, R.J. Sahani, W.L. Yen and G.W. Tautfest, Phys.Rev. 164, 1699 (1967).

6) J.A. Poirier, N.N. Biswas, N.M. Cason, I. Derado, V.P. Kenney, W.D. Shephard and E.H. Synn, Phys.Rev. 163, 1462 (1967).

7) Orsay-Milano-Berkeley Collaboration, Nuovo Cimento 53A, 798 (1967).

8) F. Schweingruber, M. Derrick, T. Fields, D. Griffiths, L.G. Hyman, R.J. Jabbur, J. Loken, R. Ammar, R.E.P. Davis, W. Krofac and J. Mott, Phys.Rev. 166, 1317 (1968).

9) Aachen-Berlin-CERN-London (I.C.)-Vienna Collaboration, Nuclear Physics B5, 567 (1968).

10) B.D. Hyams, W. Koch, D. Pellett, D. Potter, L. Von Lindern, E. Lorenz, G. Lütjens, U. Stierling and P. Weilhammer, Physics Letters 24B, 634 (1967).

11) K. Gottfried and J.D. Jackson, Nuovo Cimento 34, 735 (1964).
J.D. Jackson, J.T. Donohue, K. Gottfried, R. Keyser and B.E.Y. Svensson, Phys.Rev. 139B, 428 (1965).

12) P.V.C. Hough and B.W. Powell, Nuovo Cimento 18, 1184 (1960).

13) L. Griffiths, C.R. Symons and B. Zacharov, CERN 66-17 (1966).

14) K. Gottfried and J.D. Jackson, Nuovo Cimento 33, 309 (1964).

15) E. Malamud and P.E. Schlein, Phys.Rev. Letters 19, 1056 (1967).

16) J. Pišút and M. Roos, CERN Preprint TH.885 (1968) (to be published in Nuclear Physics).

Table 1

Density matrix elements for the reaction $\pi^- p \to \pi^- \pi^+ n$ with $|t| < 0.4$ (GeV/c)^2

$m(\pi^+\pi^-)$ (GeV)	$\lvert t'(\pi^+\pi^-)\rvert$ (GeV/c)^2	$\rho_{00}-\rho_{11}$	ρ_{1-1}	Re ρ_{10}	Re ρ_{0s}	Re ρ_{1s}
0.6 - 0.96	0.00 - 0.02	0.480 ± 0.058	0.000 ± 0.016	-0.124 ± 0.020	0.255 ± 0.029	-0.077 ± 0.012
"	0.02 - 0.05	0.525 ± 0.043	-0.020 ± 0.016	-0.180 ± 0.016	0.270 ± 0.025	-0.067 ± 0.010
"	0.05 - 0.11	0.514 ± 0.045	0.016 ± 0.019	-0.166 ± 0.019	0.238 ± 0.027	-0.064 ± 0.012
"	0.11 - 0.40	0.417 ± 0.052	0.059 ± 0.029	-0.165 ± 0.020	0.116 ± 0.029	-0.029 ± 0.014
0.30 - 0.49	0.00 - 0.20	-0.077 ± 0.102	0.005 ± 0.043	-0.104 ± 0.033	0.152 ± 0.044	-0.123 ± 0.024
0.49 - 0.59	"	0.088 ± 0.105	-0.057 ± 0.037	-0.134 ± 0.031	0.258 ± 0.040	-0.122 ± 0.023
0.59 - 0.67	"	0.374 ± 0.072	0.000 ± 0.026	-0.121 ± 0.026	0.255 ± 0.037	-0.074 ± 0.016
0.67 - 0.73	"	0.442 ± 0.055	-0.052 ± 0.020	-0.208 ± 0.021	0.211 ± 0.032	-0.081 ± 0.014
0.73 - 0.77	"	0.578 ± 0.055	0.021 ± 0.021	-0.174 ± 0.022	0.255 ± 0.033	-0.062 ± 0.014
0.77 - 0.81	"	0.520 ± 0.055	0.023 ± 0.021	-0.158 ± 0.022	0.196 ± 0.033	-0.075 ± 0.014
0.81 - 0.89	"	0.516 ± 0.054	0.003 ± 0.021	-0.148 ± 0.022	0.167 ± 0.033	-0.038 ± 0.013
0.89 - 1.11	"	0.355 ± 0.085	-0.013 ± 0.024	-0.071 ± 0.029	0.209 ± 0.042	-0.044 ± 0.015

Table 2

Masses, widths and cross-sections of ρ^0 for the reaction $\pi^- p \to \rho^0 n$ with $|t| < 0.4$ (GeV/c)^2 resulting from fits of several Breit-Wigner and background functions

	Formula	Data	Confidence $P(\chi^2)$	m_0	Γ_0	Background area [%] from 290-910 MeV	σ_1 [μb]	σ_2 [μb]
A	$\left\{ a + c \cdot \frac{1}{q} \frac{m_0 \cdot m \cdot \Gamma^*(m)}{(m_0^2-m^2)^2 + m_0^2 \cdot \Gamma^{*2}(m)} \right\} \cdot PS$	Weighted data with $\lvert t\rvert<0.4$ (GeV/c)^2	77%	775±3	145± 9	16%	109±2	123± 3
A′	$\left\{ a + c \cdot \frac{1}{q} \frac{m_0 \cdot m \cdot \Gamma(m)}{(m_0^2-m^2)^2 + m_0^2 \cdot \Gamma^2(m)} \right\} \cdot PS$		62%	775±3	154±11	20%	106±2	154± 3
B	$a + b \cdot m + c \cdot \frac{m_0 \cdot m \cdot \Gamma^*(m)}{(m_0^2-m^2)^2 + m_0^2 \cdot \Gamma^{*2}(m)}$		73%	774±3	136±11	22%	102±9	115±11
B′	$a + b \cdot m + c \cdot \frac{m_0 \cdot m \cdot \Gamma(m)}{(m_0^2-m^2)^2 + m_0^2 \cdot \Gamma^2(m)}$		66%	773±3	136±12	27%	96±9	130±12
C	$a + b \cdot m + c \cdot \frac{\Gamma_0}{4 \cdot (m_0-m)^2 + \Gamma_0^2}$		55%	777±3	131± 7	15%	109±3	119± 3
D(**)	$a \cdot \frac{q}{D_B} \int_T^{t_{min}(m)} e^{D_B \cdot t} \cdot dt + \frac{1}{q} \cdot \frac{m^2 \cdot m_0^2 \cdot \Gamma^{*2}(m)}{(m_0^2-m^2)^2 + m_0^2 \cdot \Gamma^{*2}(m)} \cdot \int_{t_{min}(m)}^{T} K^2(t) \cdot dt$		12%	762±3	148±11	18%	106±2	
E	$c \cdot \frac{1}{q} \cdot \frac{m_0 \cdot m \cdot \Gamma^*(m)}{(m_0^2-m^2)^2 + m_0^2 \cdot \Gamma^{*2}(m)} \cdot PS$	Projected p-wave $N(m) \cdot (\rho_{00}\ \rho_{1-1})$	37%	774±6	144±16	0		
F	$c \cdot \frac{m_0 \cdot m \cdot \Gamma^*(m)}{(m_0^2-m^2)^2 + m_0^2 \cdot \Gamma^{*2}(m)}$		39%	773±6	144±16	0		
G	$c \cdot \frac{\Gamma_0}{4 \cdot (m_0-m)^2 + \Gamma_0^2}$		0.15%	777±6	119±11	0		

(**) See Ref. (16)

$PS = \frac{\pi^2}{2 \cdot E^2 \cdot m} \cdot [(m^2 - (2 \cdot m_\pi)^2) \cdot m \cdot (E_{c.m.}^2 - (m_n + m)^2) \cdot (E_{c.m.}^2 \cdot (m_n - m)^2)]^{1/2}$: $\pi\pi$ effective mass distribution in three-body phase space

$\Gamma(m) = \Gamma_0 \cdot \left(\frac{q}{q_0}\right)^3 \cdot \frac{m_0}{m}$: mass-dependent width of a p-wave Breit-Wigner. $\Gamma'(m) = \Gamma(m) \cdot \frac{1 + \alpha^2 q_0^2}{1 + \alpha^2 q^2}$: width modified with a "form factor".

$q = \frac{1}{2}(m^2 - 4m_\pi^2)^{1/2}$: momentum of a pion in the ρ^0 rest frame. $E_{c.m.} = (m_\pi^2 + m_p^2 + 2 \cdot E_{lab(\pi^-)} \cdot m_p)^{1/2}$

The quantities m_0, Γ_0, a, b and c are free parameters in the fits, α is set to $1/2m_\pi$.

Figure Captions

Fig. 1 : Experimental arrangement. A, B, C, D, F. H, E and G are scintillation counters; S1-S8 are thin foil spark chambers.

Fig. 2 : Total energy of the $(\pi^-\pi^+)$ system.

Fig. 3 : Missing-mass distribution for the reaction $\pi^- p \to \pi^-\pi^+ n$.

Fig. 4 : Unweighted $(\pi^-\pi^+)$ mass distribution for the reaction $\pi^- p \to \pi^-\pi^+ n$ with $|t| < 0.4$ $(GeV/c)^2$.

Fig. 5 : t-dependence of the density matrix elements for the $(\pi^-\pi^+)$ mass region 600-960 MeV. The lines are predictions of the OPEA (see text).

Fig. 6 : Corrected $(\pi^-\pi^+)$ mass distribution for the reaction $\pi^- p \to \pi^-\pi^+ n$ with $|t| < 0.4$ $(GeV/c)^2$. The lines are phase-space and phase-space plus Breit-Wigner function A of Table 2. One event corresponds to a cross-section of 0.0118 μb.

Fig. 7 : Differential cross-sections, $d\sigma/dt'$, for the reaction $\pi^- p \to \pi^-\pi^+ n$. The lines are predictions of the OPEA for the $(\pi^-\pi^+)$ mass range 600-960 MeV (see text).

Fig. 8 : Total cross-section for $\pi^- p \to \rho^0 n$ versus the incoming π^- laboratory momentum. Data have been taken from references 1-7. The line is $\sigma(p_\pi) = 14.4\ p_\pi^{-2}$.

Fig. 9 : $N(m)(\rho_{00}-\rho_{11})$ as a function of $(\pi^-\pi^+)$ mass for the reaction $\pi^- p \to \pi^-\pi^+ n$. The Breit-Wigner function E of Table 2 is drawn.

Fig. 10 : Unweighted $(K^-\pi^+)$ mass distribution for the reaction $K^- p \to K^-\pi^+ n$ with $|t| < 0.4$ $(GeV/c)^2$.

Fig. 11 : Differential cross-section, $d\sigma/dt'$, for the reaction $K^- p \to K^-\pi^+ n$ with $(K^-\pi^+)$ mass in the range 790-990 MeV. The line is a prediction of the OPEA (see text).

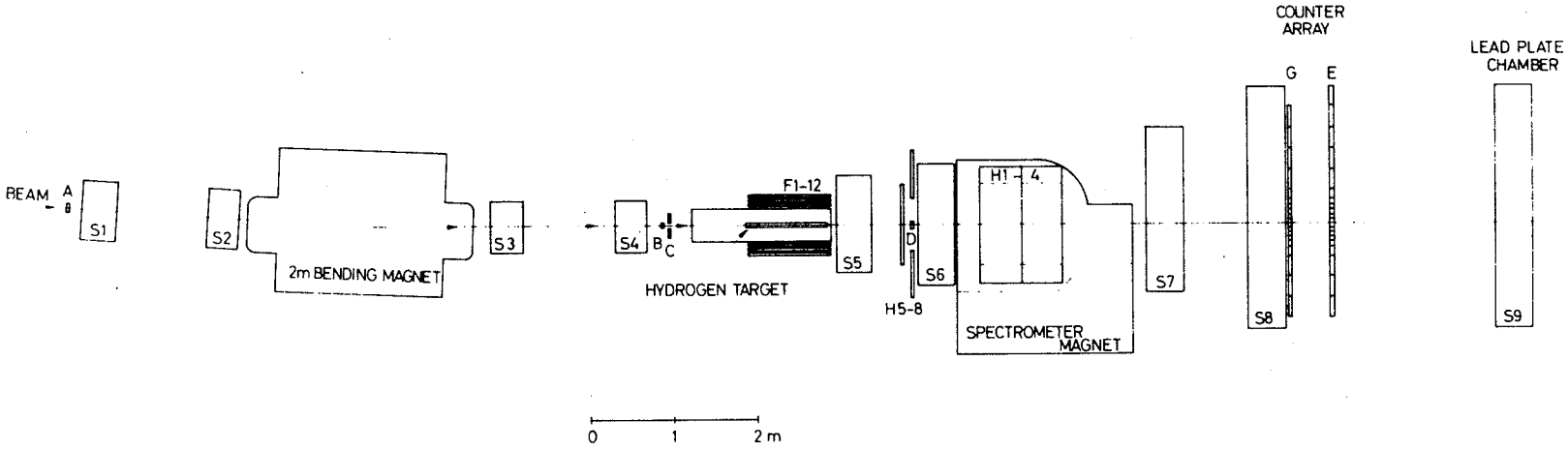
BEAM
A
B
S1
S2
2m BENDING MAGNET
S3
S4
B
C
F1-12
HYDROGEN TARGET
S5
D
S6
H5-8
H1 - 4
SPECTROMETER MAGNET
S7
COUNTER ARRAY
G
E
S8
LEAD PLATE CHAMBER
S9
0
1
2 m

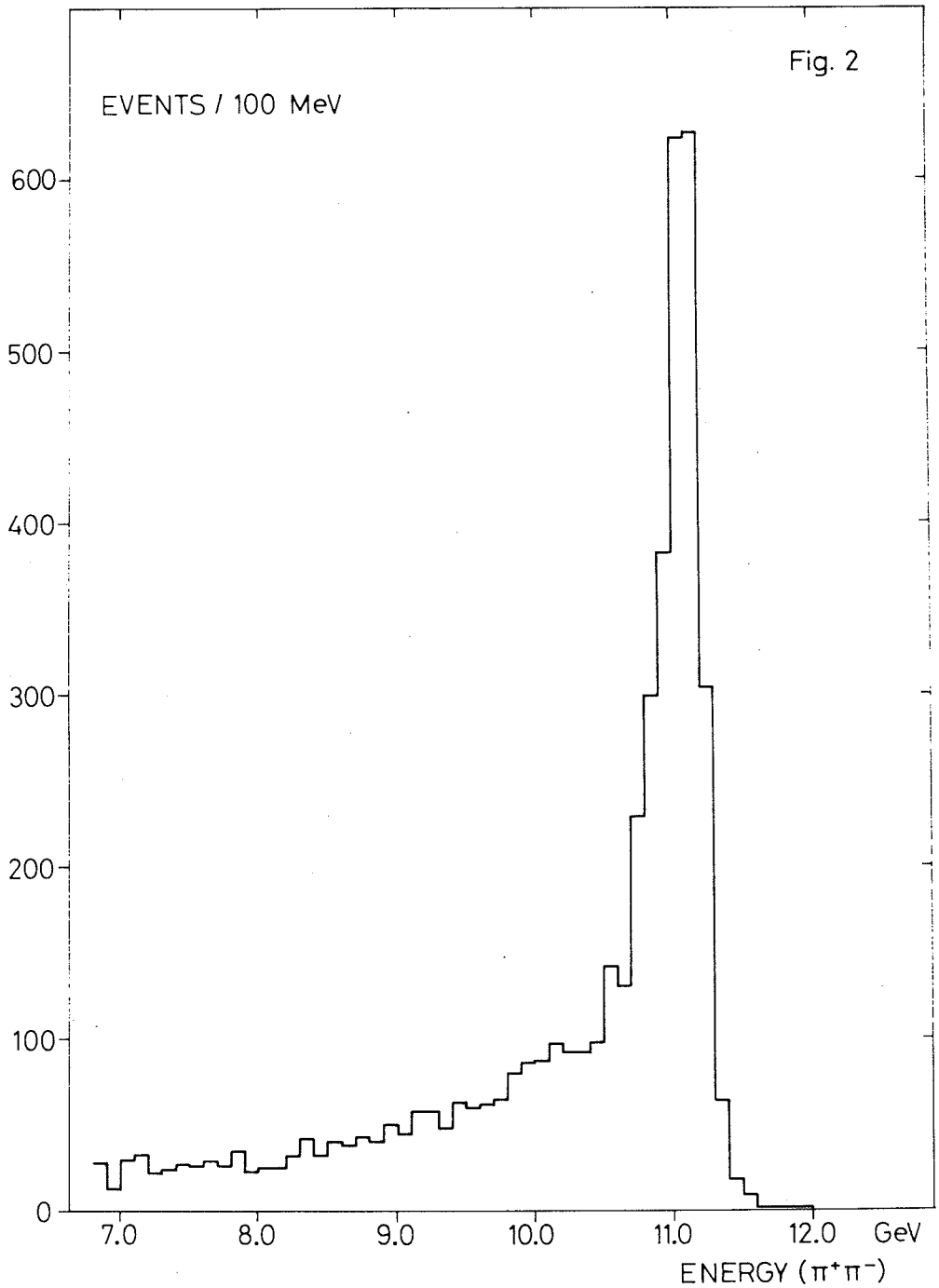
Fig. 2
EVENTS / 100 MeV
600
500
400
300
200
100
0
7.0
8.0
9.0
10.0
11.0
12.0
GeV
ENERGY (π⁺π⁻)

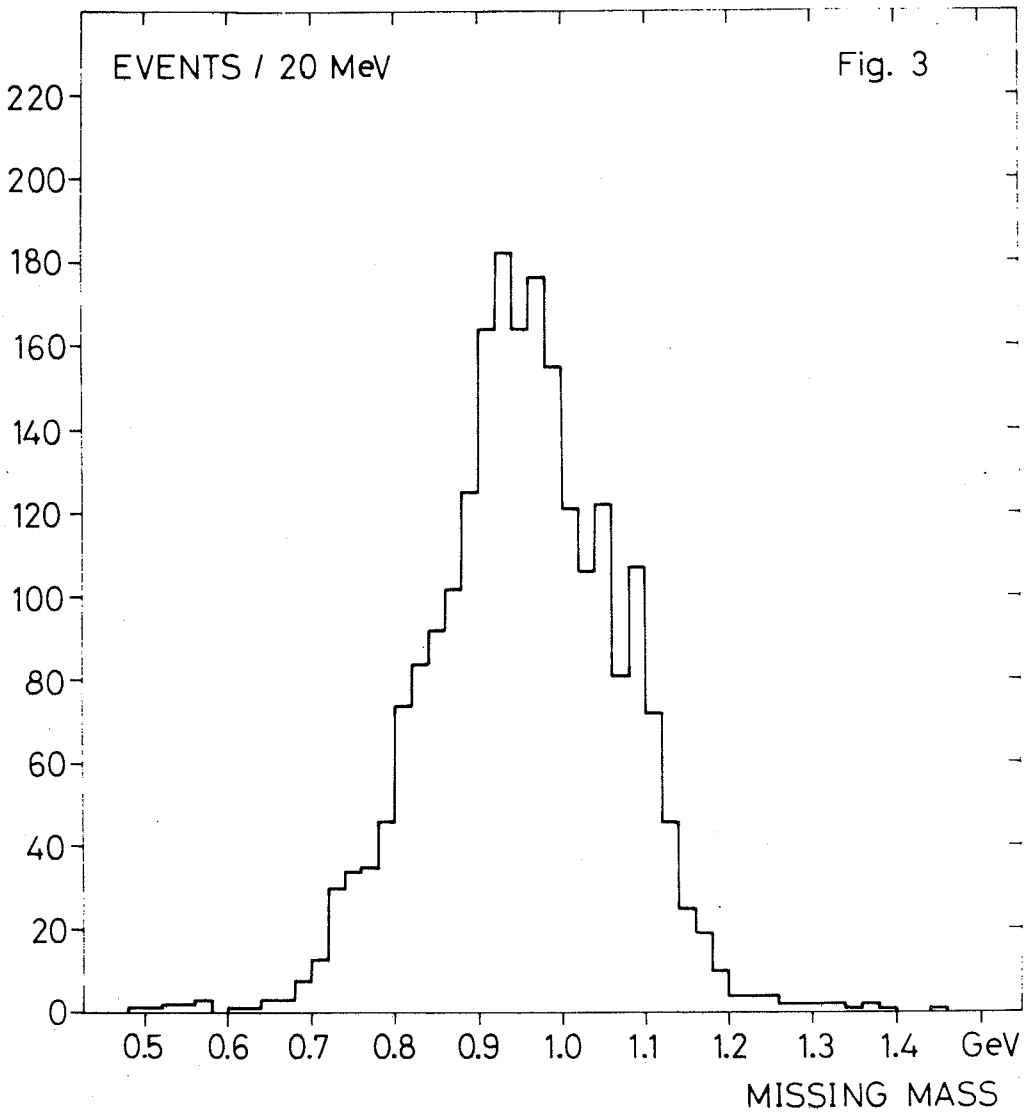
EVENTS / 20 MeV
Fig. 3
220
200
180
160
140
120
100
80
60
40
20
0
0.5
0.6
0.7
0.8
0.9
1.0
1.1
1.2
1.3
1.4
GeV
MISSING MASS

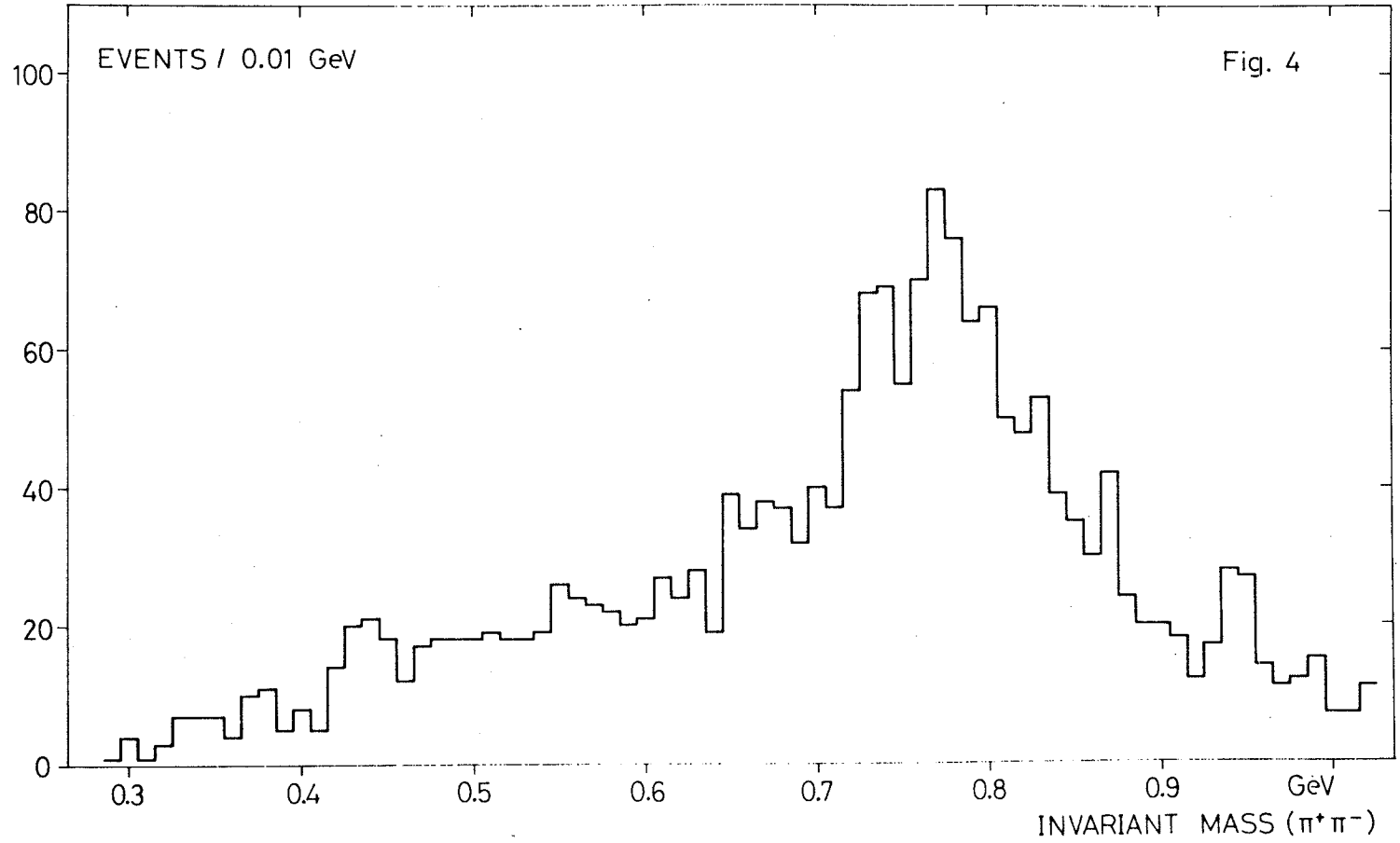
EVENTS / 0.01 GeV
Fig. 4
100
80
60
40
20
0
0.3
0.4
0.5
0.6
0.7
0.8
0.9
GeV
INVARIANT MASS (π⁺π⁻)

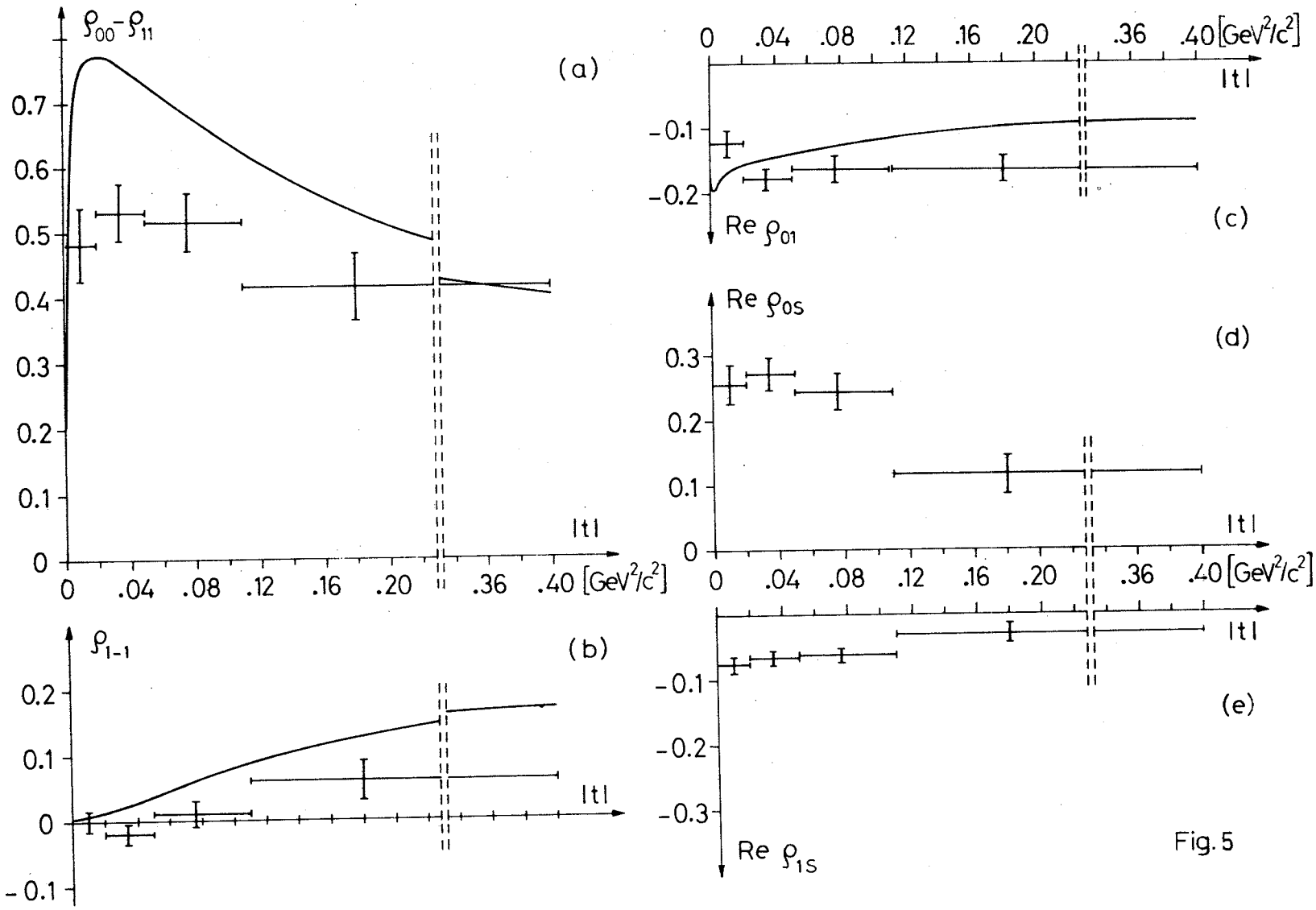
$\rho_{00}-\rho_{11}$
(a)
0.7
0.6
0.5
0.4
0.3
0.2
0.1
0
0 .04 .08 .12 .16 .20 .36 .40 [GeV²/c²]
|t|
ρ_{1-1}
(b)
0.2
0.1
0
-0.1
|t|
0 .04 .08 .12 .16 .20 .36 .40 [GeV²/c²]
|t|
-0.1
-0.2
Re ρ_{01}
(c)
Re ρ_{0s}
(d)
0.3
0.2
0.1
0
|t|
-0.1
-0.2
-0.3
Re ρ_{1s}
(e)

Fig. 5

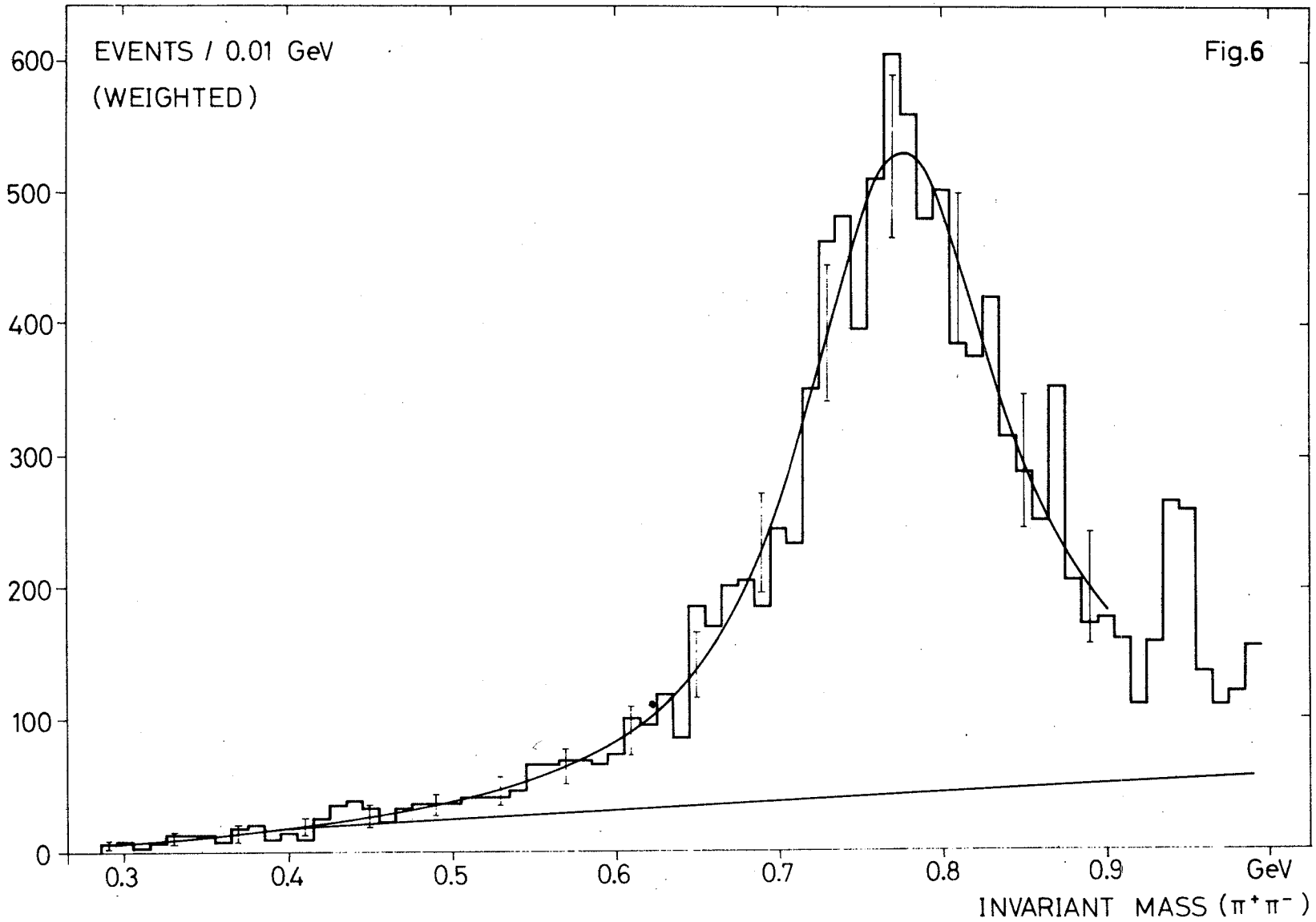
EVENTS / 0.01 GeV
(WEIGHTED)
Fig.6
600
500
400
300
200
100
0
0.3
0.4
0.5
0.6
0.7
0.8
0.9
GeV
INVARIANT MASS (π⁺π⁻)

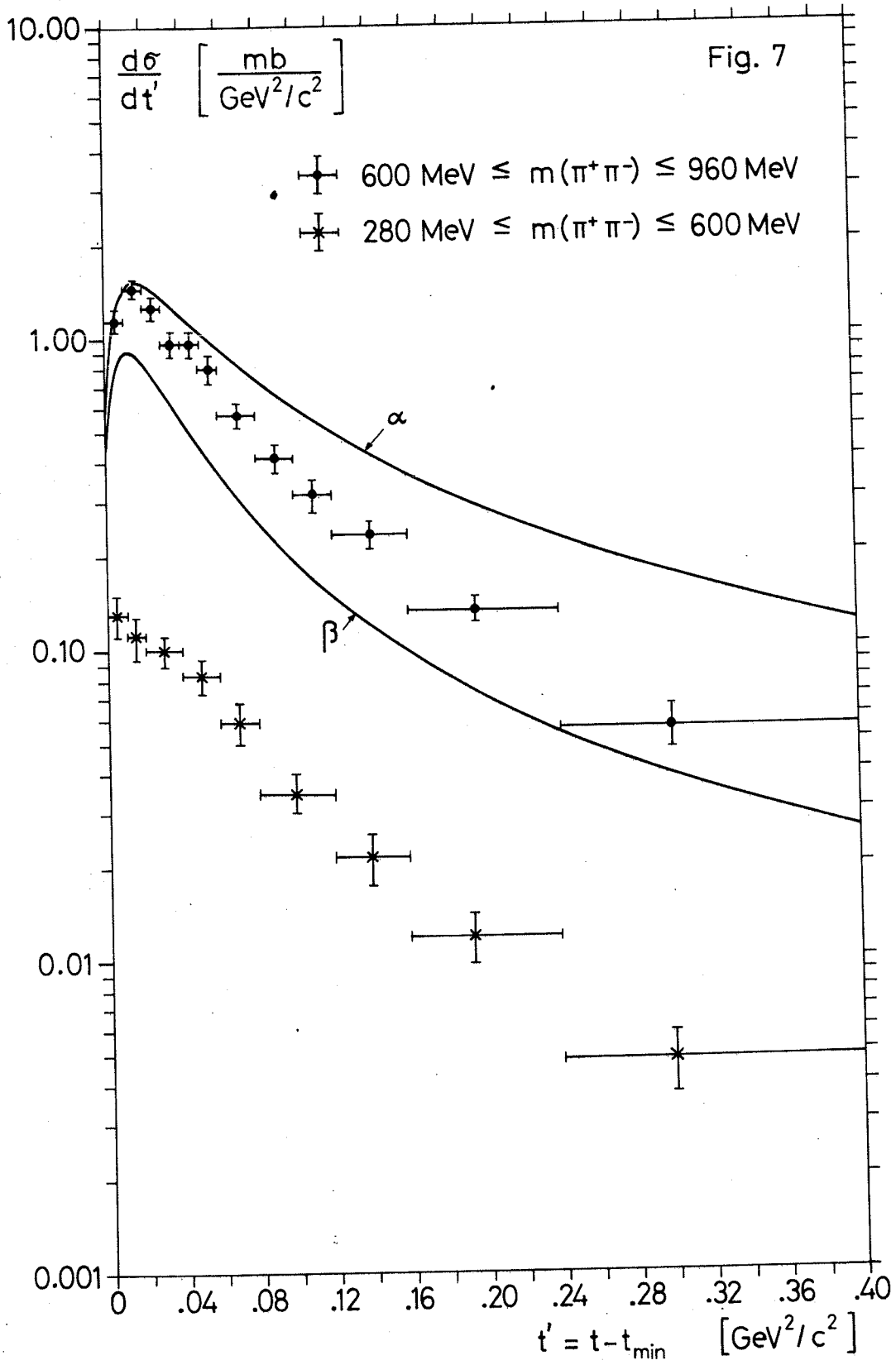
Fig. 7
dσ/dt' [mb/GeV²/c²]
600 MeV ≤ m(π⁺π⁻) ≤ 960 MeV
280 MeV ≤ m(π⁺π⁻) ≤ 600 MeV
α
β
10.00
1.00
0.10
0.01
0.001
0
.04
.08
.12
.16
.20
.24
.28
.32
.36
.40
t' = t − t_min [GeV²/c²]

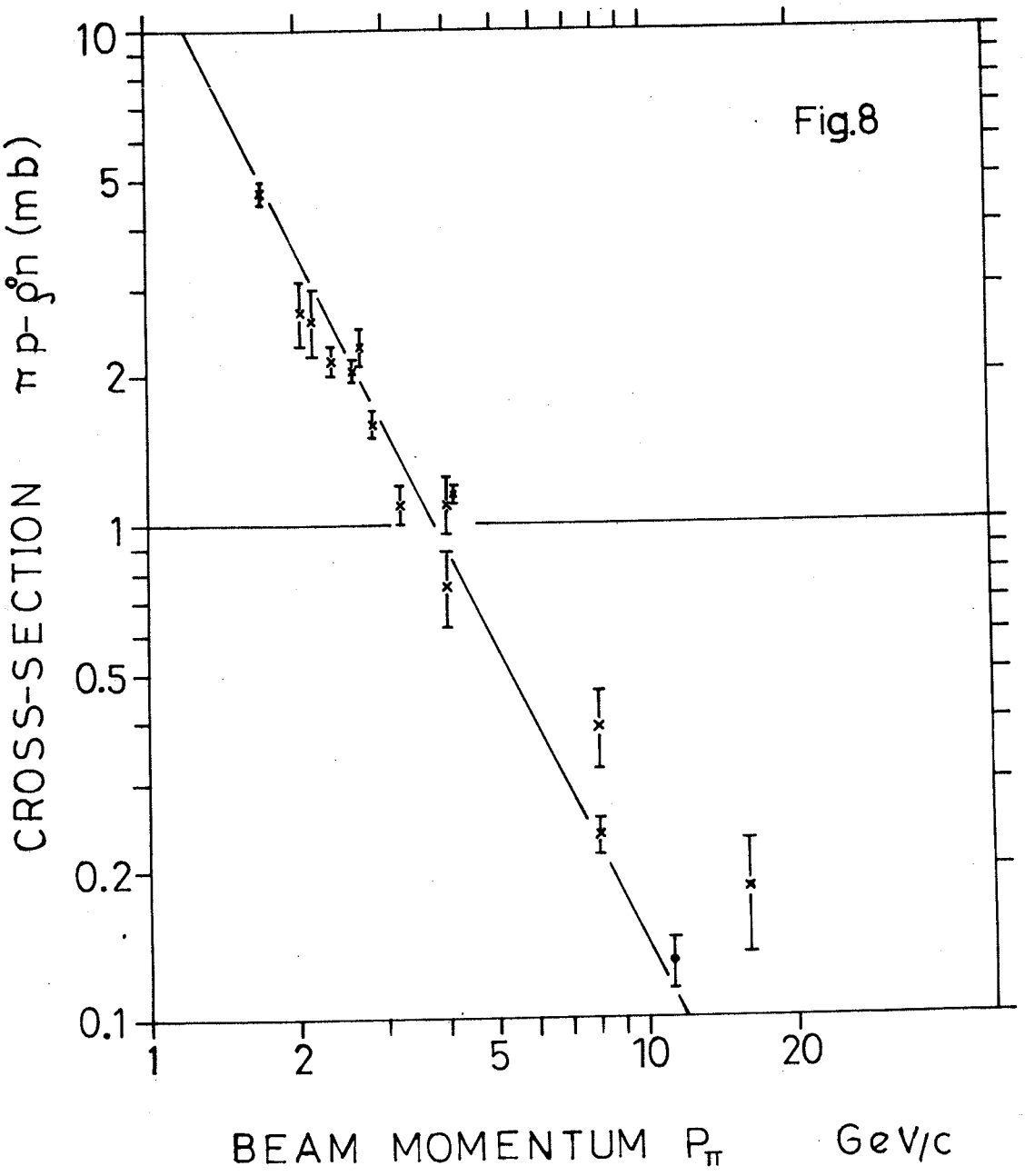
Fig.8
CROSS-SECTION π p- ρ°n (mb)
10
5
2
1
0.5
0.2
0.1
1
2
5
10
20
BEAM MOMENTUM P_π GeV/c

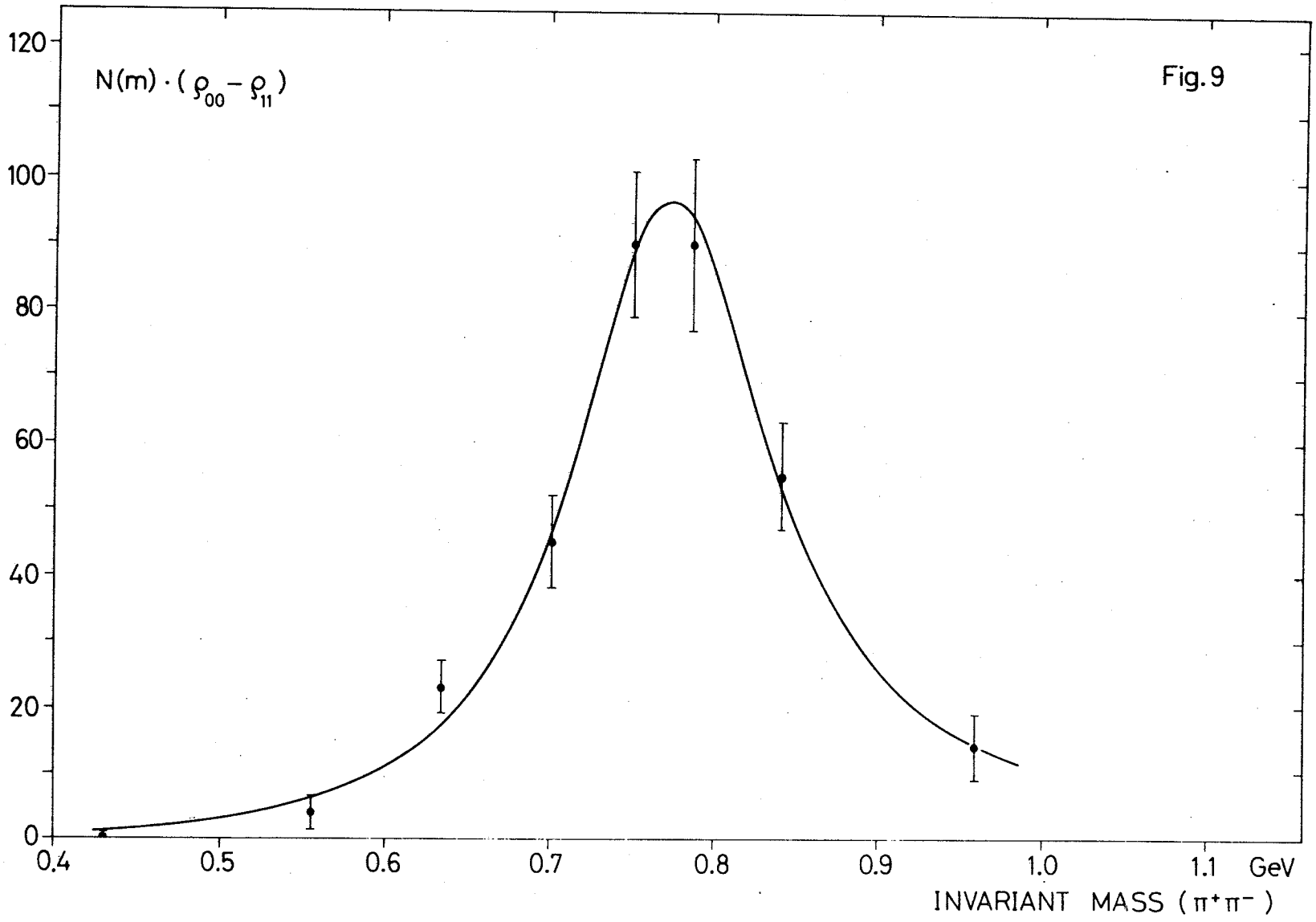
N(m) · (ρ00 − ρ11)
Fig. 9
120
100
80
60
40
20
0
0.4
0.5
0.6
0.7
0.8
0.9
1.0
1.1
GeV
INVARIANT MASS (π+π−)

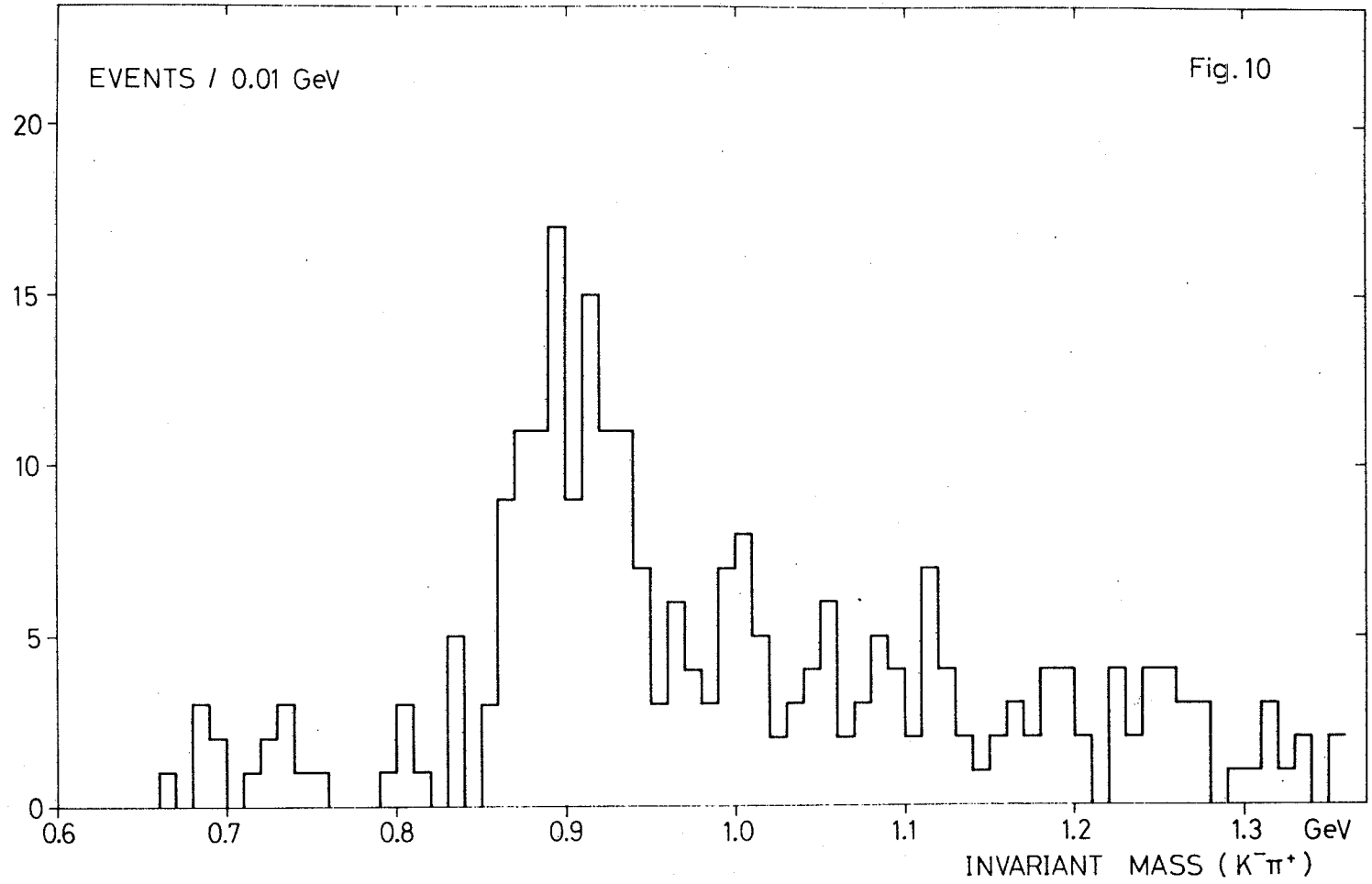
EVENTS / 0.01 GeV
Fig. 10
20
15
10
5
0
0.6
0.7
0.8
0.9
1.0
1.1
1.2
1.3
GeV
INVARIANT MASS (K⁻π⁺)

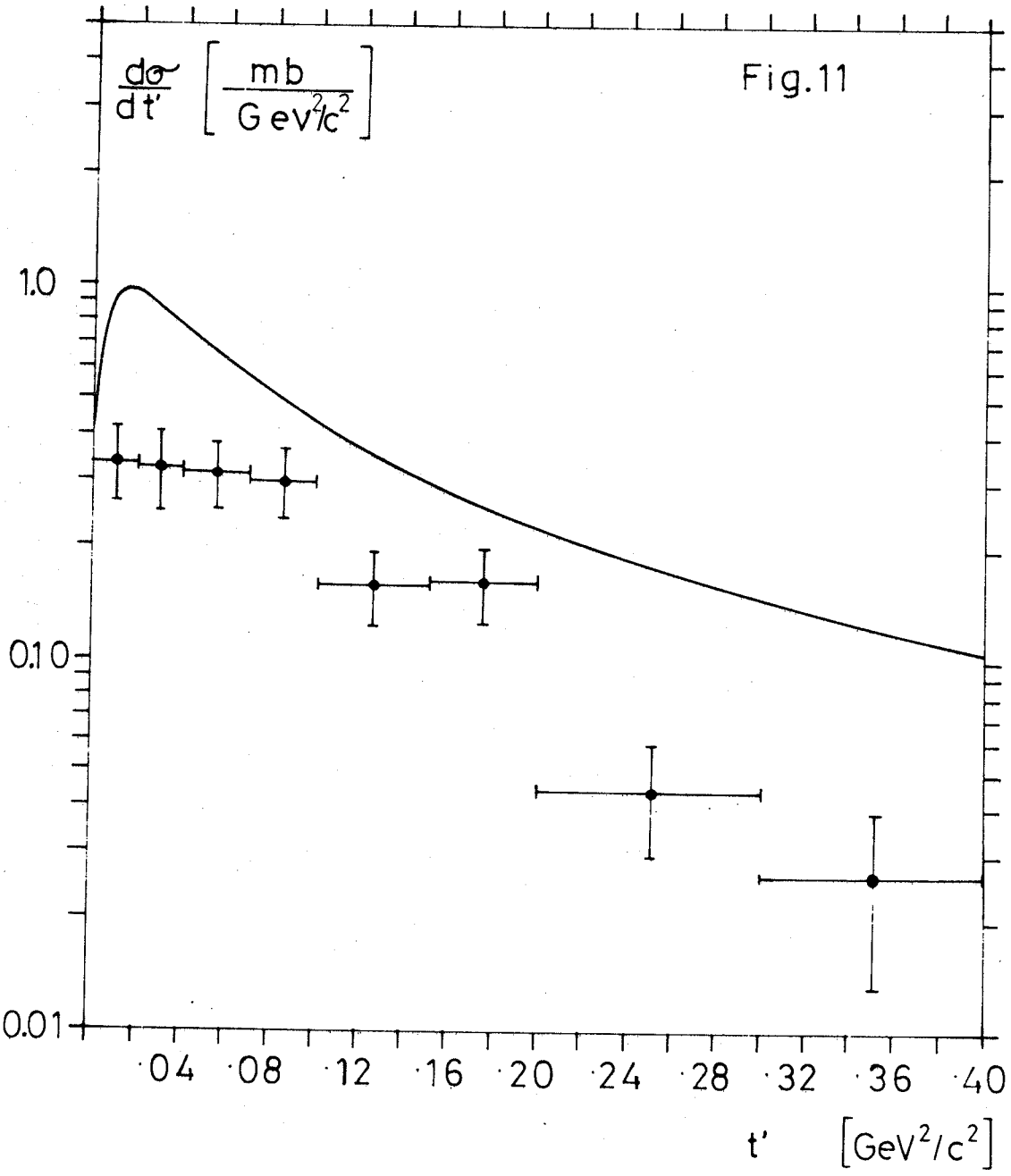
dσ/dt' [mb / GeV²/c²]
Fig.11
1.0
0.10
0.01
·04
·08
·12
·16
·20
·24
·28
·32
·36
·40
t' [GeV²/c²]